S-scheme-Mediated Ce-NSO/Ce-gCN Heterostructure for Enhanced Photocatalytic Hydrogen Evolution via Seawater Splitting

Ajeet Kumar [a], Rahul Gupta[a], Nishith Verma [a, b*]

[a] *Department of Chemical Engineering, Indian Institute of Technology Kanpur, Kanpur 208016, India.*

[b] *Center for Environmental Science and Engineering, Indian Institute of Technology Kanpur, Kanpur 208016, India.*

*Corresponding author: Prof. Nishith Verma

Tel: 91-512-259-6767, Fax: 91-512-259-0104

E-mail id: nishith@iitk.ac.in, vermanishith@gmail.com

S1. Materials and methods

Materials

Experiments were carried out using chemicals of high analytical purity. Melamine ($C_3H_6N_6$), titanium isopropoxide ($C_{12}H_{28}O_4Ti$), chloroplatinic acid solution (H_2PtCl_6) and Cerrous nitrate hexahydrate($Ce(NO_3)_3 \cdot 6H_2O$) were sourced from Sigma Aldrich (Mumbai, India). Nickel nitrate hexahydrate ($Ni(NO_3)_2 \cdot 6H_2O$), isopropyl alcohol (IPA), tert-butyl alcohol ($C_4H_{10}O$), stannic chloride hexahydrate ($SnCl_4 \cdot 6H_2O$), terephthalic acid ($C_6H_4(COOH)_2$), ammonium oxalate monohydrate ($(COONH_4)_2 \cdot H_2O$), and p-benzoquinone ($C_6H_4O_2$) were sourced from Loba Chemical Pvt. Ltd. (Mumbai, India). Ammonia solution was procured from Finar-Actylis (Gujarat, India). Simulated Seawater was prepared using NaCl, $MgCl_2$, $MgSO_4$, $CaSO_4$, K_2SO_4, K_2CO_3, and $MgBr_2$ procured from sigma Aldrich.

Materials Characterization

The synthesized materials were characterized using a range of techniques to evaluate their physicochemical properties. X-ray diffraction (XRD) was carried out with a PANalytical X'Pert^3 Powder diffractometer (USA) to identify the crystal structures of the constituent elements. Measurements were taken over the 2θ range 10 - 100° at 3°/min scan rate. Field emission scanning electron microscopy (FESEM) using the Mira3 instrument from TESCAN (USA) was used to study the surface morphology. Elemental composition was analyzed using energy dispersive X-ray spectroscopy (EDX) on the JSM-7100F JEOL system (USA). Transmission electron microscopy (TEM) and high-resolution TEM (HRTEM), performed using FEI-Tecnai G2 12 Twin and FEI Titan G2 60-300 instruments (USA), respectively, were used for detailed internal structural analysis and elemental mapping. TEM and HRTEM images were recorded at the accelerating voltages of 120 and 300 kV, respectively. Brunauer-Emmett-Teller (BET) surface areas were determined using the AS1-C Quantachrome system (USA). X-ray photoelectron spectroscopy (XPS) with the PHI 5000 VersaProbe II (FEI Inc., USA) was

used to determine the oxidation states of the elements. Photoluminescence (PL) spectra were recorded using the Agilent Cary Eclipse spectrometer (USA) at an excitation wavelength of 330 nm. UV-Vis diffuse reflectance spectra (DRS) were recorded using the Agilent Cary UMS 7000 instrument (USA), with $BaSO_4$ serving as the reference.

S1.1. Photoelectrochemical and optical measurements

S1.2. UV-Vis diffuse reflectance spectra (DRS) : UV-Vis DRS were recorded using the Agilent Cary UMS 7000 instrument (USA). The photocatalyst powder were uniformly spread on a sample holder, and the spectra were recorded using a spectrophotometer equipped with the integrating sphere, with $BaSO_4$ as the reference material. The recorded reflectance spectra were used to construct Tauc plots from which the optical band gap energy of the photocatalyst was estimated.

S1.3. Electron paramagnetic resonance (EPR) spectroscopy: Reactive oxygen species were detected by EPR spectroscopy using 5,5-dimethyl-1-pyrroline-N-oxide (DMPO) as the spin-trapping agent. For the detection of $^{\bullet}OH$ radicals, the photocatalyst was dispersed in an aqueous ethanol solution containing DMPO, while for the detection of $^{\bullet}O_2^-$, methanol solution containing DMPO was used as the solvent. The suspensions were irradiated under visible light, and the EPR spectra were recorded using the EPR spectrometer (ESR FA200, JEOL) to identify the characteristic DMPO -$^{\bullet}OH$ and DMPO -$^{\bullet}O_2^-$ adduct signals.

S1.4 Kelvin probe force microscopy (KPFM): KPFM measurements were performed using the MFP-3D Origin (Asylum Research, Oxford Instruments) system to determine the surface potential of the photocatalyst. The photocatalyst was dispersed in an isopropyl alcohol, ultrasonicated for 10 min, and drop-cast on a clean silicon wafer, which was dried at room temperature (~25 ^{o}C). The surface potential mapping was carried out under both dark and visible-light irradiation to evaluate the charge transfer behavior of the photocatalyst.

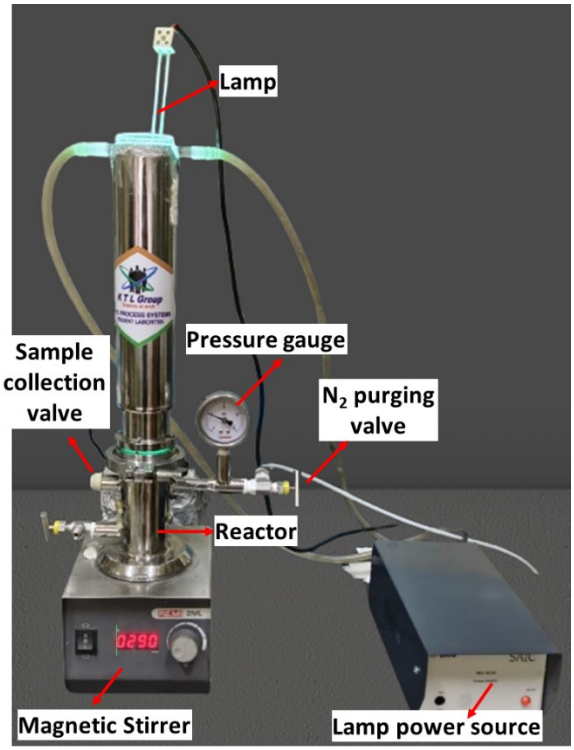

Fig. S1. Digital photograph of the photoreactor setup.

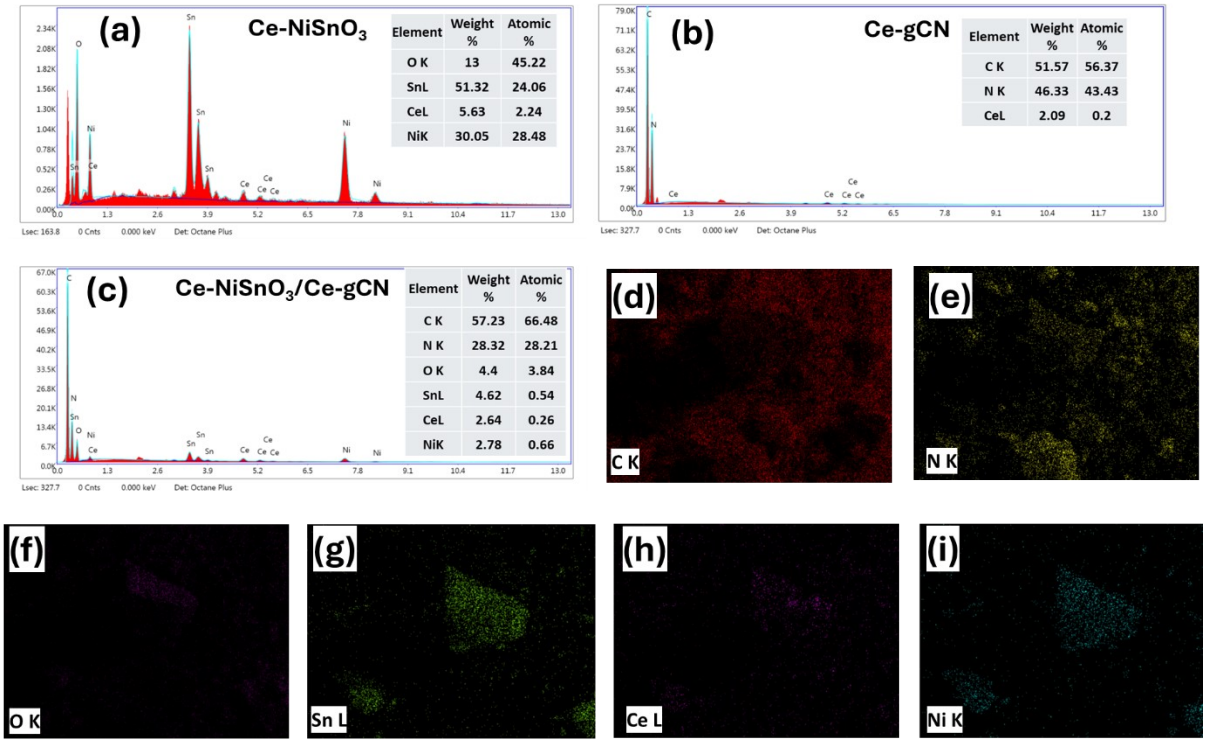

Fig. S2. (a-c) SEM-EDX spectra and the corresponding elemental distribution Ce-NSO, Ce-gCN, and Ce-NSO/Ce-gCN, respectively. (d-i)Elemental mapping of Ce-NSO/Ce-gCN.

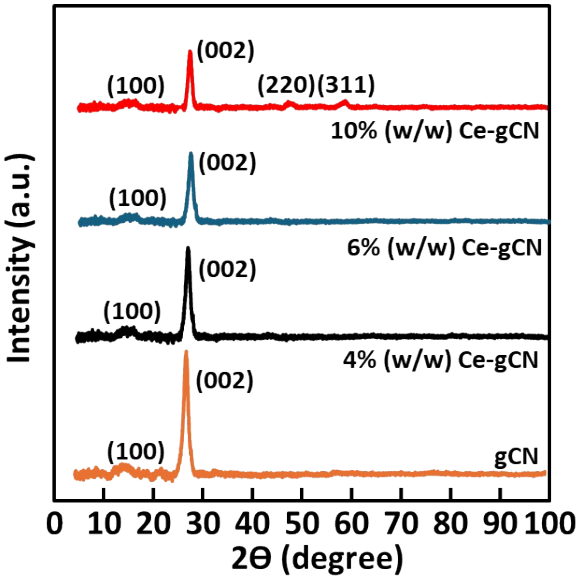

Fig. S3. XRD patterns of Ce-gCN with different Ce-loadings (0, 4, 6, and 10 % w/w).

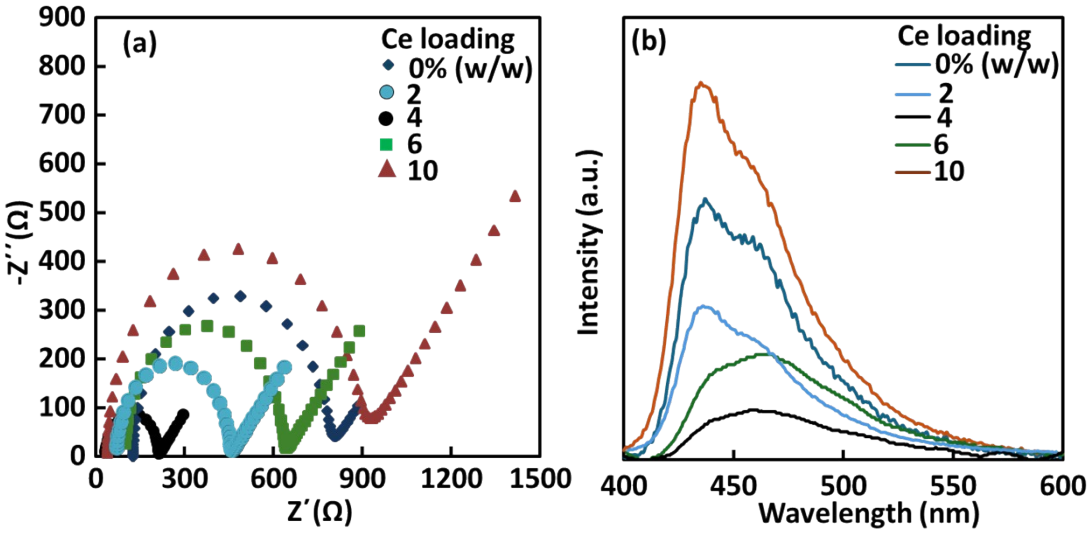

Fig. S4. (a) EIS Nyquist plots and (b) PL spectra of Ce-NSO/Ce-gCN with 0-10% Ce-loading.

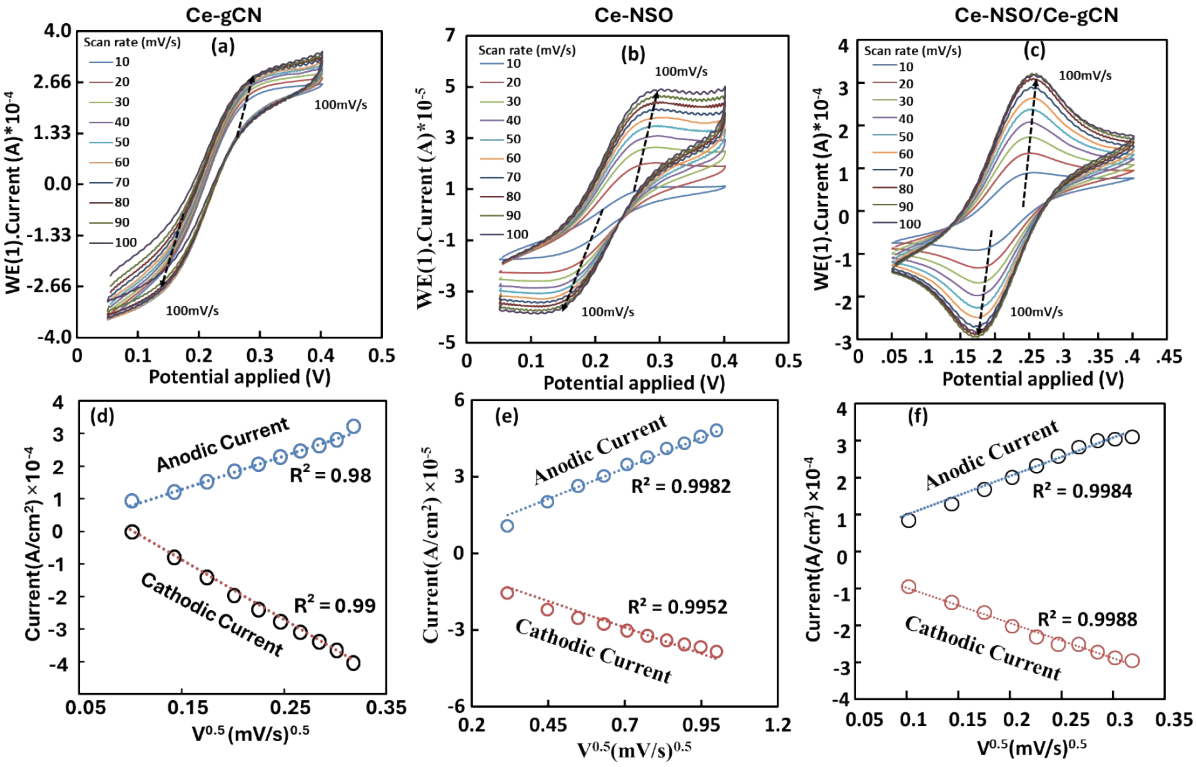

Fig. S5. (a-c) Current vs. voltage curve of Ce-gCN, Ce-NSO, and Ce-NSO/Ce-gCN, respectively; (d-f) Graph between the current and square root of scan rate for Ce-gCN, Ce-NSO, and Ce-NSO/Ce-gCN, respectively.

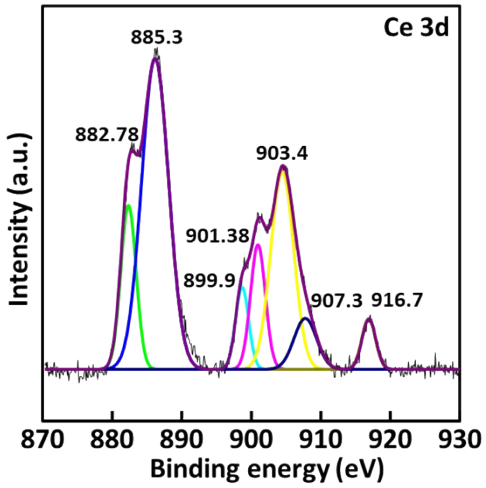

Fig. S6. Ce 3d XPS spectra of Ce-NSO/Ce-g-CN, showing the characteristic Ce^{3+} and Ce^{4+} peaks.

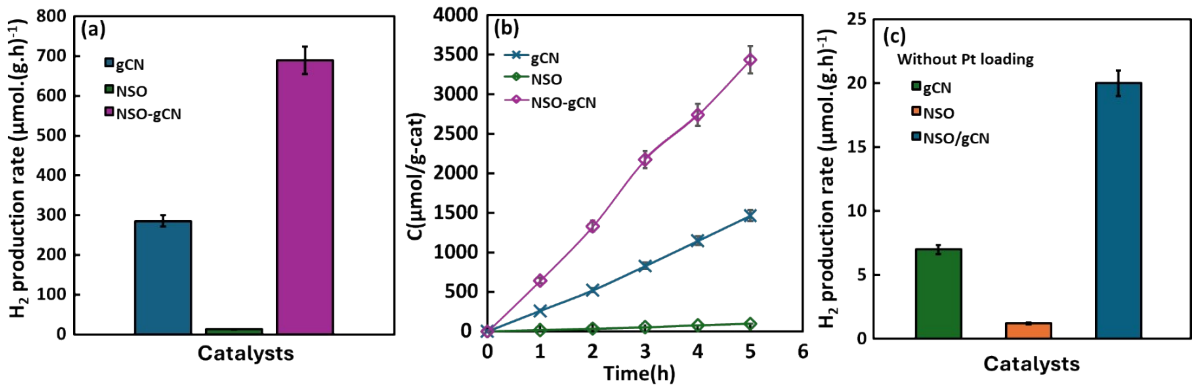

Fig. S7. (a) H_2 production rate for gCN, NSO, and NSO/gCN, with Pt (b) hydrogen concentration vs. time for gCN, NSO, and NSO/gCN with Pt, and (c) H_2 production with time over gCN, NSO, and NSO/gCN without Pt.

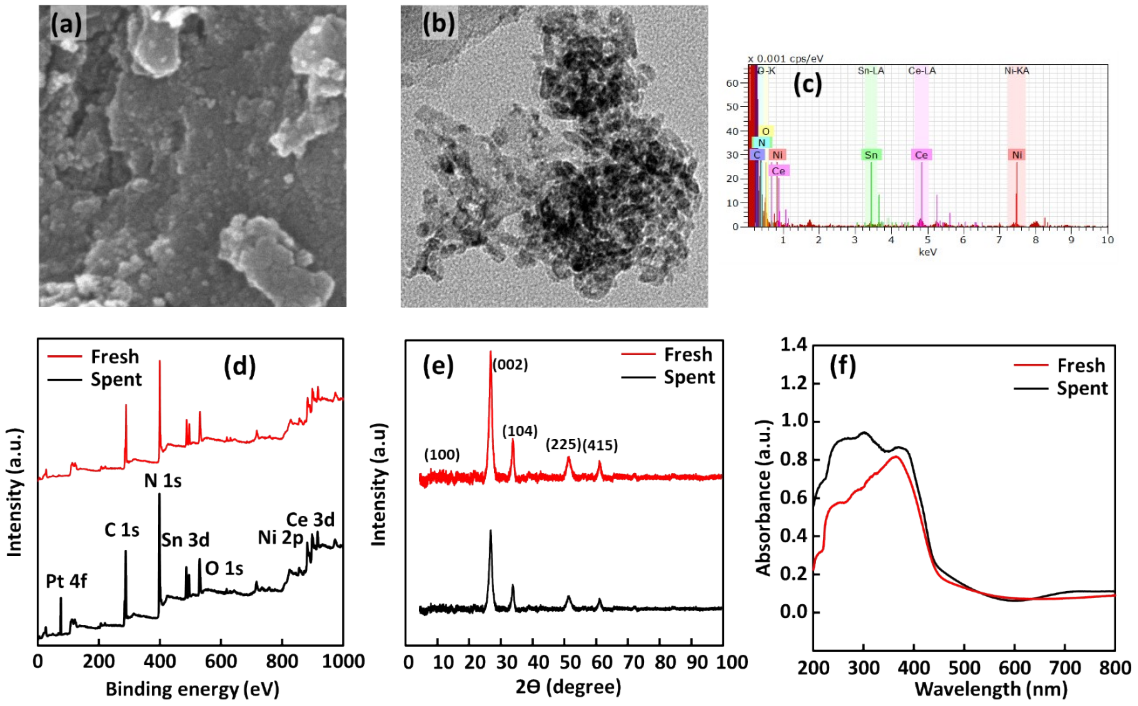

Fig. S8. (a) SEM and (b) TEM images, (c) TEM-EDX spectra of the spent Ce-NSO/Ce-gCN sample; (d) XPS survey scan, (e) XRD patterns, and (f) UV-vis DRS of the fresh and spent Ce-NSO/Ce-gCN samples.

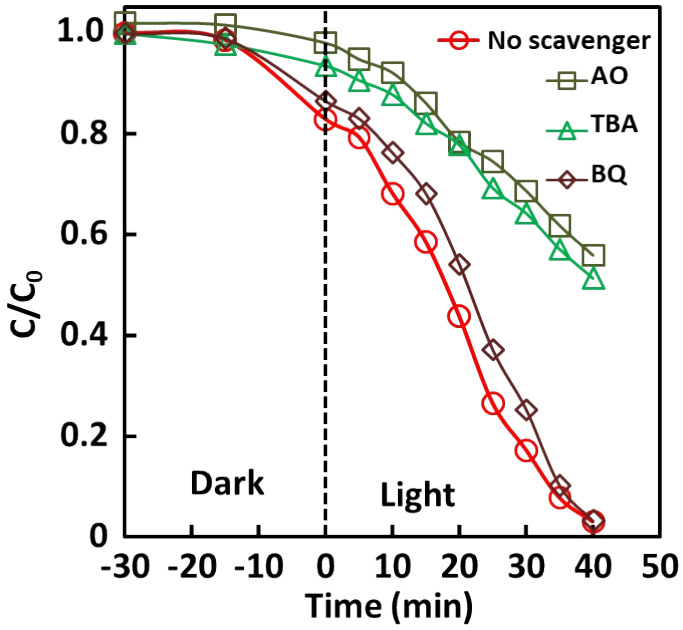

Fig. S9. Radical scavenging test data for the model RhB dye using Ce-NSO/Ce-gCN.

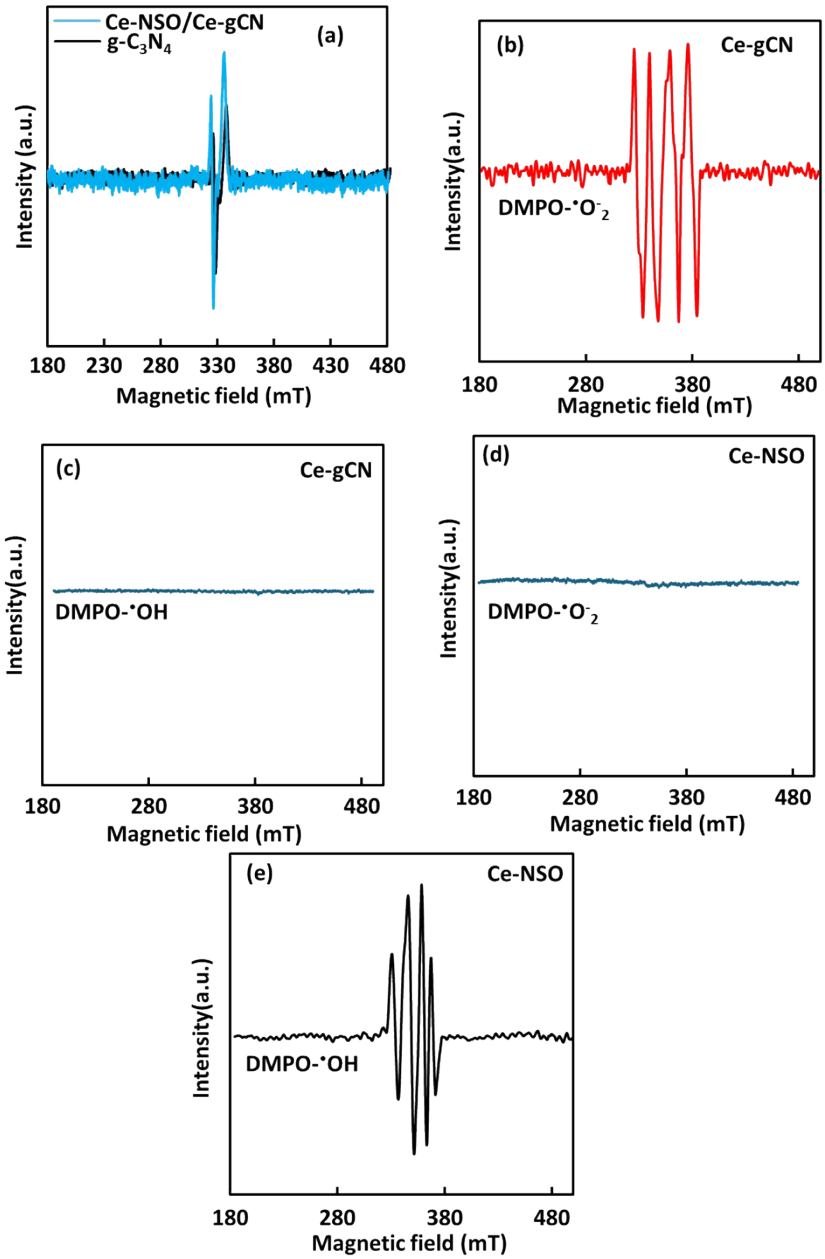

Fig. S10. (a) Solid-state EPR spectra of Ce-gCN and Ce-NSO/Ce-gCN. EPR signals of (b) DMPO-•O_2^-, (c) DMPO-•OH adducts for Ce-gCN, and (d) DMPO-•O_2^- (e) DMPO-•OH, adducts for Ce-NSO.

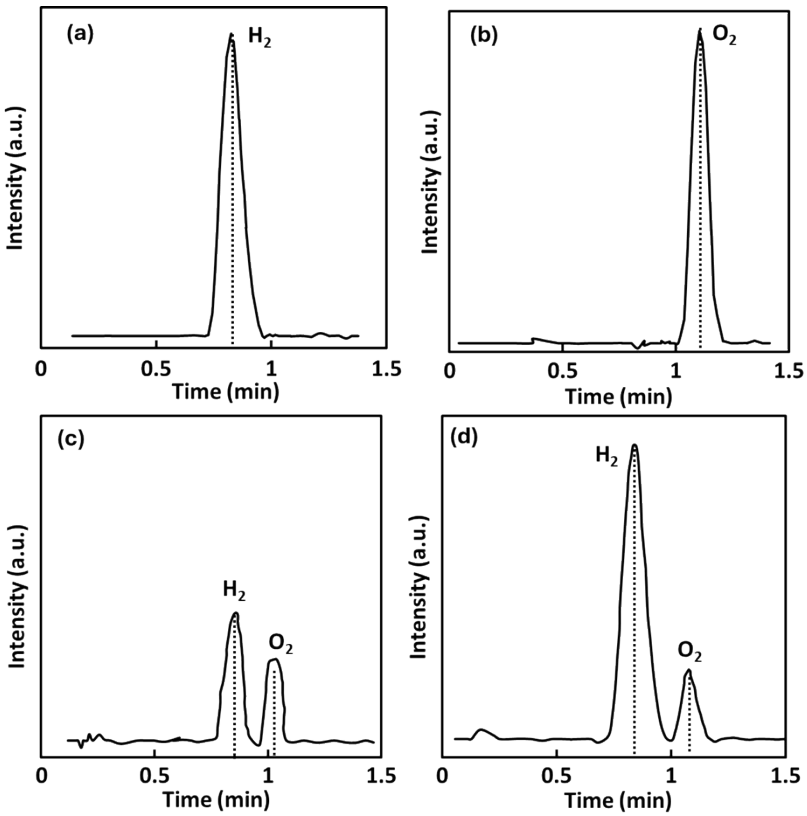

Fig. S11. GC chromatogram of pure (a) hydrogen gas, (b) oxygen gas, and (c) and (d) gas samples collected at 1 and 4 h, respectively.

Table S1. EIS data measured for different catalysts.

Catalyst	**R_s(Ω)**	**R_{ct}(Ω)**	**C(μF)**	**W(Ω)**
Ce-gCN	50	445	1.54	520.19
Ce-NSO	40	2700	28	260.5
Ce-NSO-Ce-gCN	30.6	210	9.3	105.76

Table S2. TRPL analysis showing fitted decay parameters, carrier lifetimes (τ), and average lifetime constants of the photocatalysts.

Sample	**τ_1 (ns)**	**τ_2 (ns)**	**τ_3 (ns)**	**B_1**	**B_2**	**B_3**	**$\tau_{Average}$ (ns)**
NSO-gCN	1.69	6.13	0.3	0.45	0.14	0.41	1.76
Ce-NSO/Ce-gCN	2.18	6.55	0.52	0.51	0.17	0.31	2.42

Table S3. ECSA values for the prepared photocatalysts.

Materials	**ECSA (cm^2/cm^2)**
Ce-gCN	0.521
Ce-NSO	0.315
Ce-NSO/Ce-gCN	0.689

Table S4. A comparison of the H_2 evolution efficiency of Ce-NSO/Ce-gCN with that of the photocatalysts with/without Ce-doping, reported in the literature. Studies 2-6 pertain to Ce-doped photocatalysts used for HER, however, in DI water. The next listed (7-14) studies pertain to the photocatalysts without Ce-doping, however, tested in seawater, natural or simulated.

S. No.	Photocatalysts	Preparation method	Lamp	Water source	Rate ($\mu mol.(g.h)^{-1}$)	h^+ Scavenger	CB	VB	BG	Ref.
1.	Ce-NSO/Ce-gCN	Ultrasonication-calcination	250 W visible lamp	Simulated seawater	1510	-	Ce-NSO/Ce-gCN			**This study**
							0.10 /-1.21	2.74/1.66	2.54/2.79	
2.	Ce-ZnO/CNTs	Hydrothermal	300 W Xe lamp	deionized water	759	Methanol	-0.91	2.17	3.08	[50]
3.	Ag-Ce-TiO_2 NTs film	Electrochemical	300 W Xe lamp and high-pressure Hg lamp	deionized water	1.47 ($\mu mol.cm^2.h^{-1}$)	Ethanol	-	-	3.2	[51]
4.	Ce-UiO-66/ZnCdS	Microwave irradiation	300 W Xe lamp	deionized water	3958	$Na_2S.9H_2O$ and Na_2SO_3	Ce-UiO66/ZnCdS			[52]
							-	-	2.75/2.53	
5.	Ce-$BiVO_4$/$SrTiO_3$	Hydrothermal	40 W incandescent lamp	deionized water	~154 (771.3 $\mu mol.g^{-1}$ in 5 h)		Ce-$BiVO_4$/ $SrTiO_3$			[53]
							0.197/1.43	2.52/1.79	2.33/3.22	
6.	Ce-doped ZnO/ZnS	Hydrothermal	UV lamp	3 M NaCl (aq.)	~1500	Na_2S and Na_2SO_3	-	-	2.78	[54]
7.	CuO/TiO_2	Impregnation & calcination	300 W Xe lamp	Simulated seawater	~4.8	-	-	-	3.26	[55]
8.	Ni/$La_2Ti_2O_7$	Hydrothermal	400 W Hg arc lamp	Seawater	696/598	-	-	-	2.714	[31]
9.	$(Ga_{1-x}Zn_x)(N_{1-x}O_x)$	Heating precursors in ammonia	450 W Hg lamp	Simulated seawater	333	-	-	-	2.68	[56]

10.	CDs-CdS nanosheets*	Electrolytic and solvothermal	AM 1.5 G solar simulator	Seawater	4640	Lactic acid	-	-	2.30	[57]
11.	WO_2/Na_xWO_3	Reduction	1000 W Xe	Simulated seawater	~6	-	WO_2/Na_xWO_3			[58]
							-0.7/0.7	-0.1/2.7	0.6/2.0	
12.	Brookite TiO_2 nanoparticles	Emulsification	500 W Hg lamp	Seawater	1476	-	-	-	2.72	[59]
13.	$W_{0.7}T_5C$/PCN	Solvothermal	Visible	Seawater	985	TEOA	$W_{0.7}T_5C$/PCN			[60]
							-0.87/1.57	-1.14/1.39	2.44/2.53	
14.	Pt/TiO_2	Photo-deposition	400 W Hg lamp	Seawater	300	Ethanol/ NaCl	-			[61]